Research Article

Received: 1 May 2025 Revised: 23 June 2025 Published online in Wiley Online Library:

(wileyonlinelibrary.com) DOI 10.1002/jctb.70015

Vanadium removal and recovery from aqueous solution with repeated use of a KOH-modified seaweed biochar adsorbent: characterisation and removal mechanisms

Bashir M Ghanim,[a,b] Ronan Courtney,[a,c] J Tony Pembroke,[a,d] James J Leahy,[a,d] Thomas F O'Dwyer[a,d] and John G Murnane[e*]

Abstract

BACKGROUND: Vanadium (V) is a critical raw material which is extensively used in metallurgical, aerospace and chemical industries. However, V-enriched wastewaters pose risks to human and environmental health due to their tendency to persist and bioaccumulate. Active V treatment processes generate significant quantities of byproducts with associated high operating costs and there is a need therefore to investigate novel passive technologies such as biosorption. This study investigates the capacity and reusability of KOH-modified seaweed biochar (BC_{KOH}) to (re-)adsorb, desorb and recover V, and evaluates the influences of initial V concentration, contact time, solution temperature and pH.

RESULTS: The maximum uptake of 48.8 mg V g^{-1} BC_{KOH} occurred within 75 min and followed an exothermic adsorption process best described by the Langmuir isotherm model. The magnitude of enthalpy change suggested a physisorption binding interaction with optimum uptake in the range pH 3.5–4.5. Introduction of a saline content (100–400 mg Na^{+} L^{-1}) into the adsorption solution resulted in a modest reduction in the V adsorption level by BC_{KOH} but further increases in saline concentration thereafter had only limited impact. Successive V(V) adsorption/desorption cycles indicated that V(V) binding to BC_{KOH} displays effective reversibility with the adsorbent material demonstrating good regeneration characteristics.

CONCLUSION: BC_{KOH} offers clear potential to be used as a cost-effective passive and robust adsorbent of V within a range of acidic industrial waste streams. The capacity of the biochar to desorb and re-adsorb demonstrates high V recovery potential and excellent biochar regeneration capability.

Keywords: seaweed biochar; vanadium; adsorption; desorption; recovery; regeneration

INTRODUCTION

Vanadium, even in trace amounts, promotes the synthesis of chlorophyll and the absorption of potassium and assimilation of nitrogen, thus improving the growth of plants. However, large quantities in soils (>30 mg kg^{-1}) can be toxic to animals (including humans) and plants, largely due to its ease of mobility from soil to plant roots.[1] Industrially, the vast bulk of vanadium usage is in the steel and allied industries but also has applications in catalytic, pigment, medical, battery, aerospace, chemical and metallurgical industries.[2,3] In the first instance, approximately 88% of global V use is extracted from vanadium–titanium (V–Ti) magnetite ores. China, the leading global producer and seller of vanadium products, extracts vanadium from titanomagnetite ores where V_2O_5 is the final product. The amount of resulting hazardous wastewater produced after vanadate precipitation (AVP wastewater) is approximately 2 000 000 tons per year.[4]

Vanadium in wastewaters is considered a risk to the human and environmental health due to its tendency to persist and bioaccumulate.[5,6] The mobility and, hence, toxicity of vanadium is largely a function of factors such as vanadium compound type, vanadium

* *Correspondence to: JG Murnane, School of Engineering, University of Limerick, Limerick, Ireland. E-mail: john.murnane@ul.ie*

a *Bernal Institute, University of Limerick, Limerick, Ireland*

b *Department of Medical Laboratories, The Higher Institute of Medical and Technical Sciences, Tripoli, Libya*

c *Department of Biological Sciences, University of Limerick, Limerick, Ireland*

d *Department of Chemical Sciences, University of Limerick, Limerick, Ireland*

e *School of Engineering, University of Limerick, Limerick, Ireland*

oxidation state therein and wastewater pH. The most common oxidation states for V are III, IV and V, with the latter being the most soluble and toxic form.[7,8] V(V) has been shown to be strongly soluble under oxic conditions and can display a range of surface interactions including complexation with the organic and inorganic components of sediments as well as uptake into flora and fauna.[9,10] Specific sources of V in wastewater can include highly acidic residual filtrates from steel slag processing[11] and highly basic leachate solutions from bauxite residues.[12] Typical V concentrations can range from 1 to 5 mg L^{-1} in the case of bauxite residue leachate to 200 mg L^{-1} for steel slag filtrate wastewater.[12,13] Consequently, there is a primary need to treat these waste streams not alone for the purpose of environmental protection but also as a potential source of vanadium recovery and reuse.[14,15]

Traditional methods for the treatment and recovery of vanadium from wastewaters can vary from microbiological treatment,[16,17] chemical precipitation[18] and solvent extraction[19] to membrane filtration processes.[20] All these techniques possess both advantages and disadvantages. Microbial treatment tends to produce significant sludge output, chemical precipitation requires the input of additional chemicals, solvent extraction is highly dependent on pH control, while membrane filtration requires a relatively high setup cost.[21]

Research efforts are now beginning to focus on the use of adsorption as a means of recovering vanadium from its waste waters. Adsorption and adsorbents offer several advantages including variety of adsorbent types, possibility of selectivity towards specific metal ions of interest along with the possibility of adsorbent regeneration and metal recovery and all through a relatively straightforward process.[22] Recent research studies have focused on the use of a range of adsorbent-type materials for V recovery and these can be largely classified into resins, minerals and biosorbents. Resin-type adsorbents such as Amberlite IRA-400 chelating resin[23] and a weak base resin D314[24] have been successfully employed for V(V) removal. Mineral-based adsorbents mostly based around iron have also proven useful in the removal of V(V) from waste solutions with significant uptake levels being achieved on both a commercial CFH-12 adsorbent[25] and a layered double hydroxide-supported nanoscale zerovalent iron.[26] Recent research outlines the desire for transformation of natural feedstocks into high-performance carbon adsorbents and biosorbents.[27,28] Biosorbents have also been employed in V(V) removal such as the use of a biochar-stabilised nano zero-valent iron,[29] waste crab shells,[30] quaternary ammonium-modified surfaces of pine bark[31] and red mud-modified sawdust biochar.[12] While the use of biochars as adsorbents for a variety of heavy metals has been researched including the use of pineapple leaf biochar for Ni, Zn and Cu removal,[32] the removal of Pb, Cu and Ni using a *Vetiveria zizanioides*-derived biochar[33] and competitive removal of a series of heavy metals using a peanut shell-derived biochar,[34] there exists a limited number of studies specifically in relation to V(V) removal. These include the biosorption of V(V) onto a H_3PO_4-modified *Lantana camara* biochar[35] and the use of urea- and thiourea-modified pine bark biochar.[36] More recently, natural marine materials, including seaweed waste and seaweed-derived biochars, are seen as effective low-cost adsorbents for V(V) removal due in large part to their abundance of surface functional groups. However, research on their modification and application in environmental remediation remains limited.[37]

The aim of the study reported here was to prepare a potassium hydroxide (KOH)-modified seaweed biochar (BC_{KOH}) and assess its capacity for the removal of V(V) from aqueous solutions. Key objectives were to establish the mechanisms of adsorption, to investigate the influence of solution pH, initial V(V) concentration, temperature and ionic strength, and to evaluate the reversibility of the adsorption process.

EXPERIMENTAL

Materials

Seaweed (*Ascophyllum nodosum*) samples were collected on the southwest coast of Ireland and stored at room temperature in sealed polyethylene bags. Aqueous solutions of potassium metavanadate, potassium hydroxide, sodium hydroxide and sodium chloride were made up by dissolution of each salt in deionised water. All salts, along with hydrochloric acid and nitric acid, were purchased from Sigma-Aldrich.

Adsorbent preparation

Dried seaweed (*Ascophyllum nodosum*) powder and solid KOH were thoroughly mixed at KOH/seaweed weight ratios of 1:1 and then pyrolysed in a reactor at 700 °C for 1 h under limited oxygen conditions. The resultant KOH-modified biochar (BC_{KOH}) was powdered and repeatedly washed using 1 mol L^{-1} HCl to remove KOH residues, followed by washing with deionised water until the washings attained neutral pH. For comparison, unmodified biochar (BC) was also prepared from seaweed (*Ascophyllum nodosum*) via pyrolysis under the same conditions and then washed several times with deionised water. The biochar samples (BC and BC_{KOH}) were then dried overnight at 60 °C, ground to <0.75 mm particle size, homogenised and stored for use in an air-tight container at room temperature.

Characterisation methods

Characterisation methods were conducted on a dry basis (db) using standard methods (as outlined below) with all measurements performed in triplicate.

Elemental analysis of the pre- and post-modified biochar samples (BC and BC_{KOH}) was conducted for C, H, O and N compositions using acid digestion in a microwave system according to CEN/TS 15290:2006. Ash content was measured according to BS EN 14775:2009 (550 °C). The physicochemical properties of prepared biochar samples were evaluated by BET, N_2 adsorption/desorption isotherms at 77 K using an automatic volumetric system (TriStar II Plus, Micrometrics Instrument Corporation). Investigation of the surface morphologies of the biochar samples along with their surface elemental composition were carried out using a Hitachi S-2700 scanning electron microscope (SEM) and energy-dispersive X-ray (EDX) spectroscopy respectively. Fourier transform infrared (FTIR) analysis using a Cary 630 FTIR spectrometer was employed to investigate the surface functional groups on the various biochar samples. Further analysis of the surface composition of the original or modified biochars was carried out using X-ray photoelectron spectroscopy (XPS; ESCA Lab 250Xi). All aqueous concentrations of metal ions were determined using inductively coupled plasma optical emission spectrometry (Agilent Technologies 5100).

Batch adsorption experiments

Adsorbate solution preparation

Potassium metavanadate was used to prepare 1000 mg L^{-1} stock solutions of V(V). The solutions used in subsequent experiments

Journal of Chemical Technology and Biotechnology published by John Wiley & Sons Ltd on behalf of Society of Chemical Industry (SCI).

were freshly prepared by serial dilution of the stock solutions and the pH was adjusted using 1.0 mol L^{-1} NaOH and HCl.

In each batch adsorption experiment, 25 mL of a selected V(V) pure solution was added to 50 mg of BC_{KOH} adsorbent in a 50 mL polypropylene centrifuge tube. The samples were shaken (IKA 130 Basic shaker), filtered (0.45 µm syringe filters) and measured for pH and metal ion concentrations. Each experiment was carried out in triplicate ($n = 3$). Specifically, optimum solution pH, contact time and temperature conditions for V(V) adsorption onto BC_{KOH} were determined. In determining optimum adsorption pH conditions, initial V(V) concentrations of 100 mg L^{-1} were adjusted in the range pH 2–12, mixed with 50 mg of BC_{KOH} and shaken for 24 h. In the case of optimising adsorption contact time, initial V(V) concentrations of 70 mg L^{-1}, at solution pH 4, were mixed with 50 mg of BC_{KOH} and shaken for 5–360 min. The influence of temperature on the adsorption process was established using initial V(V) concentrations (75 mg L^{-1}, pH 4), mixed with 50 mg of BC_{KOH} and shaken for 180 min in the temperature range 293–343 K.

The optimum established process parameters of pH, contact time and temperature were then used in the adsorption isotherm experiments where 25 mL of each initial V(V) solution concentration ranging from 3 to 175 mg L^{-1} (at solution pH 4 and temperature 293 K) was mixed with 50 mg of BC_{KOH} adsorbent. Each mixture was then shaken for 180 min, filtered and the resultant supernatant measured for V(V) concentrations.

Point of zero charge

The point of zero charge (pH_{pzc}) of BC_{KOH} was determined by making up 30 mL solutions of 0.05 mol L^{-1} NaCl in 50 mL centrifuge tubes ($T = 293$ K). The solution pH values were adjusted between 2 and 10 using 1.0 mol L^{-1} HCl or NaOH solution and 0.1 g samples of BC_{KOH} were then added to each tube. The suspensions were shaken at room temperature for 24 h (IKA 130 Basic orbital shaker) and the final pH of each solution measured using a SparkVue 4.1.0 pH meter. Differences between the initial and final pH values (ΔpH) were then plotted against the initial pH, where pH_{pzc} for the BC_{KOH} material was defined as the point of intersection of the resulting curve with the *x*-axis.

Ionic strength

Initial V(V) concentrations of 90 mg L^{-1} were combined with sodium chloride solutions containing 0–400 mg L^{-1} of Na^+ at a BC_{KOH} application rate of 2 g L^{-1}, pH 3.5, contact time of 180 min and temperature of 293 K. The supernatant was filtered, and V(V) concentrations were measured.

Desorption and regeneration experiments

To determine the reusability of BC_{KOH} to adsorb V(V), three consecutive desorption–adsorption cycles ($n = 3$) were carried out. Adsorption was carried out using a simulated V(V) solution (293 K, pH 4) with average initial concentration of 95 mg L^{-1}. After each cycle, the V(V)-loaded BC_{KOH} (V-BC_{KOH}) sample was mixed (*ca* 10% w/v) at room temperature with a 2 mol L^{-1} KOH desorbing agent and shaken for 2 h. The solutions were then filtered and the desorbed residue BC_{KOH} (Des-V-BC_{KOH}) was washed with distilled water until a neutral pH was reached. Des-V-BC_{KOH} was then oven-dried at 60 °C overnight before being used to repeat the adsorption process.

All batch adsorption experiments were conducted in triplicate. Adsorption capacity (q, mg g^{-1}) for V(V) removal was obtained using Eqn (1):

$$q = \frac{(C_o - C_e)}{Wt} \times V \quad (1)$$

where C_e and C_o (mg L^{-1}) are the equilibrium and the initial V(V) solution concentrations, respectively, V (L) is the volume of solution and Wt (g) is the mass of adsorbent.

RESULTS AND DISCUSSION

Characterisation

The surface area increased significantly from 97.3 m^2 g^{-1} for BC to 787.2 m^2 g^{-1} for BC_{KOH} while the pore volume also increased from 0.07 cm^3 g^{-1} (BC) to 0.63 cm^3 g^{-1} (BC_{KOH}). The pore radius increased slightly from 13.7 Å for BC to 16.1 Å for BC_{KOH} (Table 1). The measured surface area of the BC is higher than those of corn cob (54–57 m^2 g^{-1}), wheat straw (46–49 m^2 g^{-1}) and rice straw (62–63 m^2 g^{-1}), all pyrolised at 650 °C.[37] The increased surface area of BC_{KOH}, as a result of chemical activation, is comparable to that of KOH-modified balsa wood (808.7 m^2 g^{-1})[38] but lower than that of KOH-modified cedar wood (1017.2 m^2 g^{-1}).[39] The pore volume of BC is higher than that of biochar derived from pineapple leaf (0.01 cm^3 g^{-1}) and peanut shell (0.01–0.02 cm^3 g^{-1}),[32,34] while the pore volume of BC_{KOH} is comparable with that of industrial microalgae hydrochars and seaweed hydrochar (0.32–0.61 cm^3 g^{-1})[40,41] but much lower than that of red mud-modified sawdust biochar (666.3 cm^3 g^{-1}).[12] These variations in pore volume characteristics are likely due to the properties and compositions of the different materials used.

FTIR spectra from 400 to 4000 cm^{-1} for BC, BC_{KOH}, V-BC_{KOH} and Des-V-BC_{KOH} are outlined in Fig. 1. Analysis of the FTIR data reveals that all four spectra show little change and provide a somewhat limited level of information in the context of functional group presence on BC_{KOH}. Specifically, however, it appears that there is a slight broadening and increased intensity of the peak around 3300 cm^{-1} resulting from the treatment of the biochar with KOH. This can be attributed to stretching vibrations of hydroxyl groups (—O—H).[35,42] There is also a slight increase in intensity in the 1950–2300 cm^{-1} region of the spectrum on going from BC to BC_{KOH} and this may be attributable to the presence of (—C≡C—).[43] The bands at 1480 and 1560 cm^{-1} can be attributed to the asymmetric and symmetric stretching vibrations of (—C=O) or (—C=C—) groups.[44] The band centred around 1000 cm^{-1}, which perhaps shows the most significant change on KOH modification of the biochar, suggests the presence of either or both alcohol or carboxylic group stretching vibrations (—C—OH or O—C=O) on the newly modified BC_{KOH} surface.[45]

The surface morphologies and associated surface elemental compositions, as determined using SEM and EDX techniques, are displayed in Fig. 2. The ninefold increase in pore volume from BC to BC_{KOH} (Table 1) and the presence of porous structures is evident from the higher resolution images (Fig. 2(a),(b)), indicating a

Table 1. Surface area, pore volume and pore radius of BC and BC_{KOH}

Parameter	BC	BC_{KOH}
Surface area (m^2 g^{-1})	97.3	787.2
Pore volume (cm^3 g^{-1})	0.07	0.63
Pore radius (Å)	13.7	16.1

Journal of Chemical Technology and Biotechnology published by John Wiley & Sons Ltd on behalf of Society of Chemical Industry (SCI).

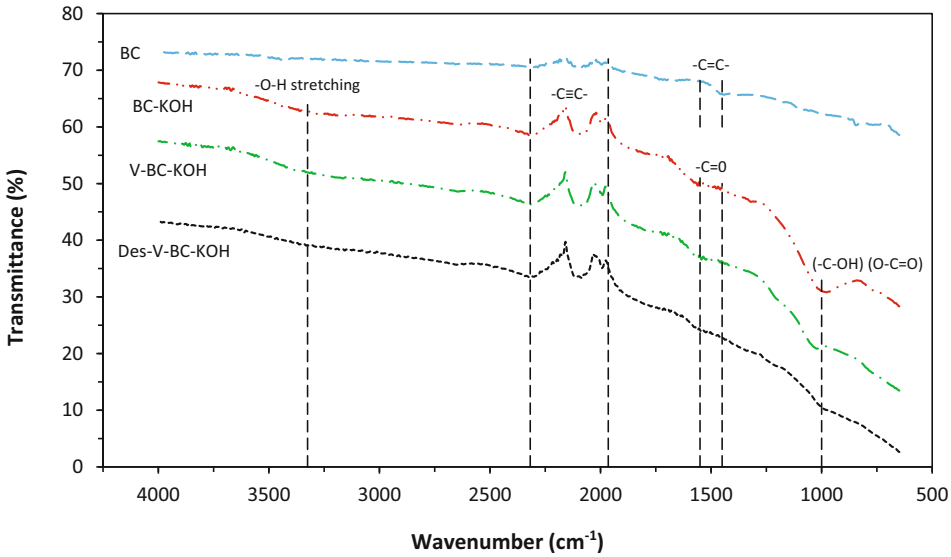

Figure 1. FTIR spectra of BC, BC_{KOH}, V-BC_{KOH} and Des-V-BC_{KOH}.

mesoporous network within the modified biochar structure. This porous structure is maintained for V-BC_{KOH} and Des-V-BC_{KOH} (Fig. 2(c),(d)).

EDX analysis indicates that carbon forms the main percentage of BC and the BC_{KOH}, followed by oxygen and with much smaller amounts of sulfur, sodium, magnesium and calcium. Further

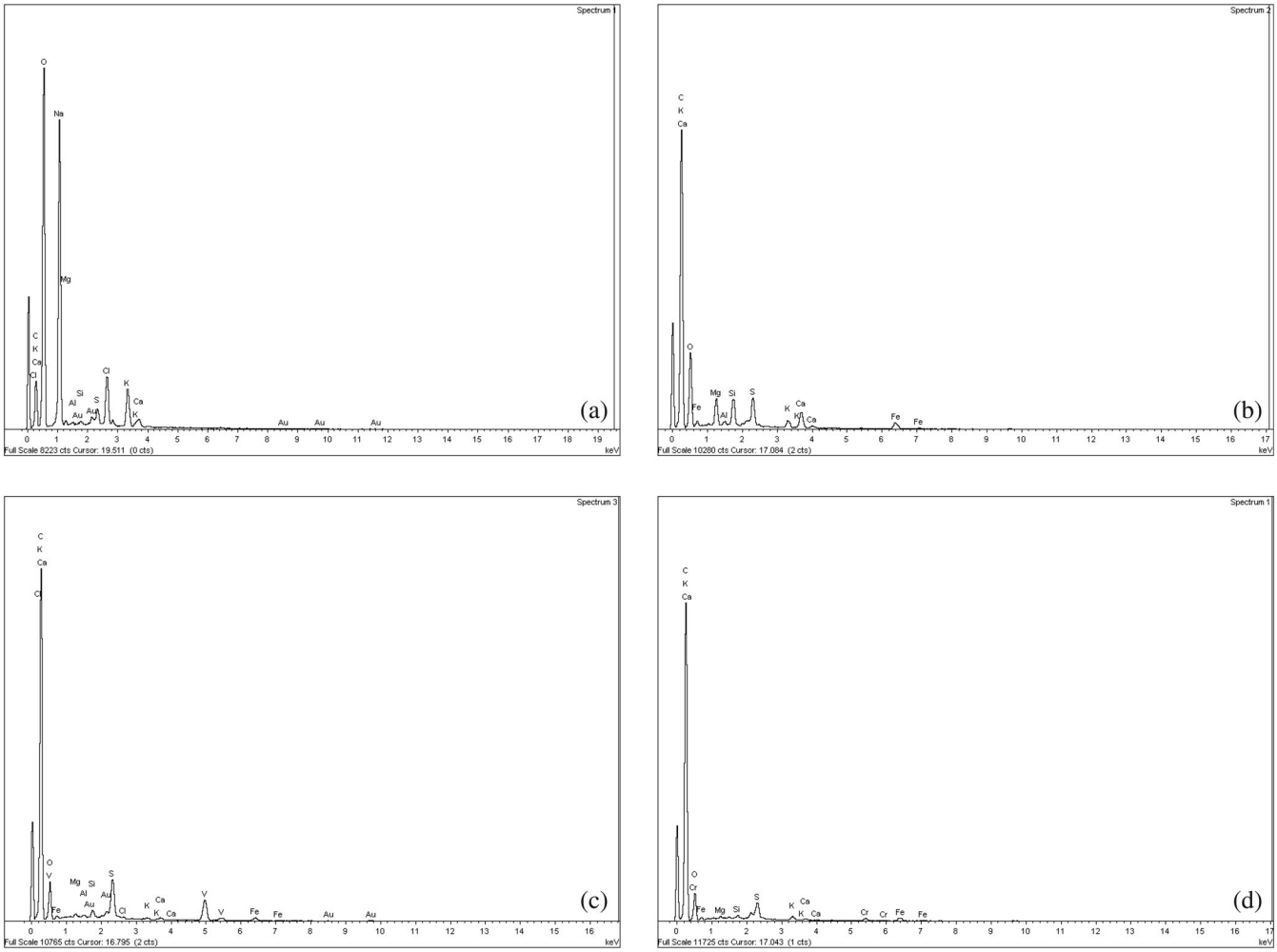

Figure 2. SEM images, EDX spectra and elemental composition of (a) BC, (b) BC_{KOH}, (c) V-BC_{KOH} and (d) Des-V-BC_{KOH}.

Journal of Chemical Technology and Biotechnology published by John Wiley & Sons Ltd on behalf of Society of Chemical Industry (SCI).

evidence from the EDX analysis also confirms the presence of V(V) on V-BC_{KOH} along with the almost complete absence of V(V) from Des-V-BC_{KOH} (Fig. 2(c),(d)), thus indicating a potentially reversible V(V) adsorption process.

The surface chemical elements of BC, BC_{KOH}, V-BC_{KOH} and Des-V-BC_{KOH} were further analysed using XPS and both the scans and surface elemental compositions are presented in Fig. 3 and Table 2 respectively. These scans provide further evidence in support of the FTIR results in relation to the formation of new surface functionality on the BC_{KOH} surface. Table 2 evidences a clear increase in the oxygen composition level in the KOH-modified biochar where the percentage composition of oxygen on the surface rises from 19.61 to 29.94 at%.

Further assessment of the specific C 1s, O 1s and V 2p regions (Fig. 4) gives a deeper insight into the modification and adsorption processes. The C 1s XPS spectrum of BC exhibited three peaks at 284.8, 286.3 and 288.7 eV corresponding to the carbon-based functional groups C–C/C–H, C–O–C and O=C–O, respectively.[46]

Following treatment of the biochar with KOH, an additional peak is observed in the BC_{KOH} scan at 287.5 eV indicating the possible formation of an additional surface-type carbonyl group (-C=O) on the BC_{KOH} surface.[47] In the case of the V-BC_{KOH} material where V(V) has been adsorbed, all four C 1s peaks continue to remain visible but there appears to be a mild downward shift of the 286.3 and 287.5 eV peaks to 286.1 and 287.4 eV, respectively, indicating the probable interaction of the adsorbed V(V) with these particular BC_{KOH} oxygenated surface moieties. The O 1s XPS spectrum of BC exhibited two peaks at 531.9 and 533.1 eV corresponding to C–O and O=C–OH, respectively.[48] Modification of BC with KOH led to formation of an extra peak in the O 1s spectrum also at 534.5 eV and this most likely corresponded to one of the following groups: C=O/C–O–H/C–O-C.[49] In a similar way, previous research has suggested that heteroatom doping based on KOH treatment of biochar leads to surface functionality improvements and a boosting of catalytic and adsorption performance.[50] With the adsorption of V(V) onto V-BC_{KOH}, all four O 1s peaks continue to remain visible but again there are mild downward shifts in the 531.9 and 533.1 eV peaks to 530.9 and 532.5 eV, respectively, also lending credence to the adsorption interaction at these sites between V(V) and the BC_{KOH} material. Further evidence of the V(V) interaction with the BC_{KOH} surface to form V-BC_{KOH} and its resultant adsorption process can be seen in the XPS analysis (Fig. 4) where the V $2p_{3/2}$ peaks at 518 and 525.2 eV are absent as would be expected from both the BC and BC_{KOH} materials but emerge in the V-BC_{KOH} spectrum (following adsorption of V(V)) and disappear again in the Des-V-BC_{KOH} spectrum (following desorption of V(V)).[49]

Influence of solution pH on V(V) removal

The effect of initial solution pH on V(V) removal by the modified biochar (BC_{KOH}) is outlined in Fig. 5(a) where it is observed that at low initial solution pH values of <2, little V(V) uptake is achieved. Increasing the initial solution pH to between 2 and 4 leads to a sharp increase in V(V) uptake with a plateau or optimal uptake range occurring between pH 3.5 and pH 4.5, where the level of V(V) uptake reaches its maximum of approximately 44 mg g^{-1} of the BC_{KOH} material. Initial solution pH > 4.5 leads to a sharp reduction in V(V) uptake by the BC_{KOH} material.

Several parameters are important in assessing the adsorption capacity of an adsorbent. These include the nature and charge associated with the surface binding groups, the adsorbent's point of zero charge (pH_{pzc}) and the influence of the adsorption solution pH on both the adsorbent surface sites and the speciated nature of the adsorbate in solution.[51] In respect of the adsorbent, the surface binding sites would be expected to be positively charged at solution pH below the pH_{pzc} and negatively charged at pH above. In the case of BC_{KOH}, the pH_{pzc} was estimated to be pH 10 for the adsorbent (Fig. 5(b)).

In solution, V(V) can exist as several speciated forms, and these vary with pH.[52-54] At low adsorption solution pH < 2 it would be expected that V(V) would exist as a positively charged VO_3^+ species. At this pH, it would also be expected that the BC_{KOH} surface

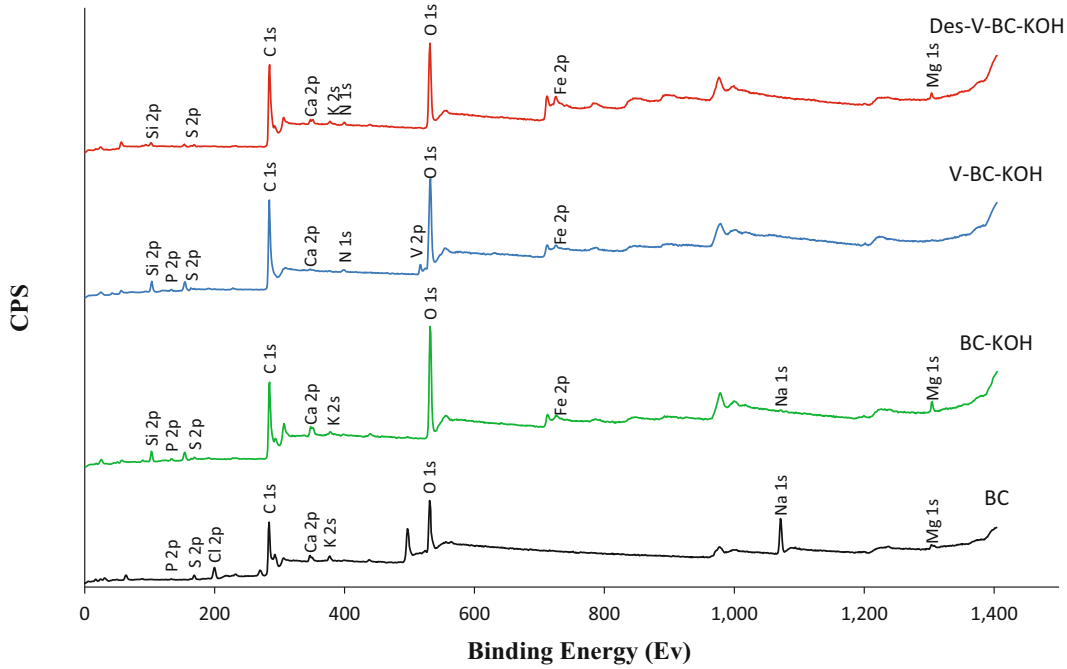

Figure 3. XPS spectra for BC, BC_{KOH}, V-BC_{KOH} and Des-V-BC_{KOH}.

Journal of Chemical Technology and Biotechnology published by John Wiley & Sons Ltd on behalf of Society of Chemical Industry (SCI).

Table 2. Atomic species and percentages for BC, BC_{KOH}, V-BC_{KOH} and Des-V-BC_{KOH}

BC		BC_{KOH}		V-BC_{KOH}		Des-V-BC_{KOH}	
Name	At (%)	Name	At (%)	Name	At (%)	Name	At (%)
O 1s	19.61	O 1s	29.94	O 1s	28.58	O 1s	25.77
C 1s	60.61	C 1s	55.50	C 1s	59.38	C 1s	62.89
Cl 2p	4.40	Mg 1s	1.69	N 1s	1.19	N 1s	0.98
Mg 1s	1.43	Ca 2p	1.97	P 2p	0.61	Mg 1s	0.90
Na 1s	7.30	Fe 2p	1.69	V 2p	0.72	Fe 2p	3.93
Ca 2p	1.62	S 2p	1.20	Fe 2p	1.44	Ca 2p	1.02
S 2p	2.38	P 2p	1.04	S 2p	0.84	S 2p	0.92
P 2p	0.43	Si 2p	5.78	Si 2p	7.01	Si 2p	2.00
K 2s	2.22	K 2s	0.95	Ca 2p	0.24	K 2s	1.58
		Na 1s	0.24				

would be positively charged and given the cationic form of V(V), coupled with a positively charged adsorbent surface, little or no adsorption of V(V) would be expected to occur as borne out in Fig. 5(a). As the solution pH rises from pH 2 to pH 4, the V(V) species changes to the anionic form $H_2VO_4^-$ and a highly significant increase in anionic V(V) adsorption onto the positively charge surface results with a maximum V(V) uptake observed at pH 4 (Fig. 5(a)). As the pH of the solution rises further from pH 4 to pH 7.5, the anionic V(V) species $H_2VO_4^-$ continues to remain dominant in solution but the positive surface charge on the BC_{KOH} reduces significantly and consequently the level of V(V) uptake reduces correspondingly as the pH rises within this range.

Kinetics

One of the most important adsorption parameters to be determined is the rate at which adsorption takes place along with determination of the rate-limiting step for that process. The adsorption kinetics of V(V) onto BC_{KOH} and associated nonlinear regression curves for the pseudo-first-order (PFO)[55] (Eqn 2), pseudo-second-order (PSO)[56] (Eqn 3) and Elovich[57] (Eqn 4) kinetic approaches are outlined in Fig. 6(a). Further assessment in relation to determination of the rate-limiting step for the V(V) adsorption onto BC_{KOH} was conducted via the intra-particle diffusion method[58,59] (Eqn 5). The coefficients of determination (R^2) and chi-squared (χ^2) values were used to assess the goodness of fit with the experimental data.

$$q_t = q_e\left(1-e^{-k_1 t}\right) \quad (2)$$

$$q_t = \frac{k_2 q_e^2 t}{1+k_2 q_e t} \quad (3)$$

$$q_t = \frac{1}{\beta}\ln(1+\alpha\beta t) \quad (4)$$

$$q_t = c_i + k_i t^{1/2} \quad (5)$$

where q_e (mg g^{-1}) and q_t (mg g^{-1}) are the adsorption capacities of V(V) at equilibrium and time t (min) respectively, and k_1 (min^{-1}) and k_2 (g mg^{-1} min^{-1}) are the kinetic constants of the PFO and PSO models respectively. The Elovich model constants α (mg g^{-1} min^{-1}) and β (mg g^{-1}) are the initial adsorption rate and the desorption constants respectively, while k_i (mg g^{-1} $min^{-1/2}$) is the intra-particle rate diffusion constant and c_i (mg g^{-1}) is the equilibrium constant related to the boundary layer thickness.[60]

Figure 6(a) indicates that the level of V(V) uptake on BC_{KOH} increased rapidly at low contact times (up to 25 min) but stabilised and plateaued thereafter suggesting that the uptake process could be divided into a fast and slow stage. In the initial faster phase of adsorption, V(V) occupies many of the available binding sites on the BC_{KOH} surface. Subsequently, the number of free binding sites diminishes and the V(V) uptake levels off after approximately 30 min. Complete equilibrium time for V(V) adsorption on BC_{KOH} was 75 min.

Both the Elovich and PSO plots show good approximation to the experimental V(V) uptake levels as a function of contact time, while the PFO model was not well fitted (lower R^2 and higher χ^2, Table 3). The Elovich model is an empirical assessment, usually used to describe physicochemical adsorption mechanisms, including where new surface interactions have been formed and it can be suggested therefore that the adsorption of V(V) onto BC_{KOH} is primarily by electrostatic attraction, with ion exchange and complexation with active sites also contributing. This supports indications from the PSO model for V(V) uptake on BC_{KOH} of at least a two-step adsorption process.[61-63] In support of this finding, the intra-particle diffusion model can then be deployed as a means of confirming the presence of two or more steps influencing the overall rate of the adsorption process.[64] The intra-particle diffusion plot can be seen in Fig. 6(b) and consists of two linear segments, the first which can be attributed to film diffusion of the V(V) adsorbate from the bulk of the adsorption solution across the film to the surface of BC_{KOH}. The second linear segment of the graph indicates a subsequent change to an intra-particle diffusion influence on the rate of V(V) adsorption. Assessment of the adsorption rate constants for both segments of the intra-particle diffusion graph (Table 3, Fig. 6(b)) indicates a more rapid film diffusion step up to about 30 min, followed by a slower intra-particle diffusion step thereafter ($k_{i1} > k_{i2}$). This suggests that intra-particle diffusion could be the rate-determining step of the adsorption process.

To further evaluate the rate-limiting step of the V(V) adsorption process, the model developed by Reichenberg[65] and Boyd[59] was applied to the experimental data. The associated equations for this model are presented as Eqns (6) and (7):

$$Bt = -\ln\frac{\pi^2}{6} - \ln(1-F(t)), \text{for } F(t) > 0.85 \quad (6)$$

Journal of Chemical Technology and Biotechnology published by John Wiley & Sons Ltd on behalf of Society of Chemical Industry (SCI).

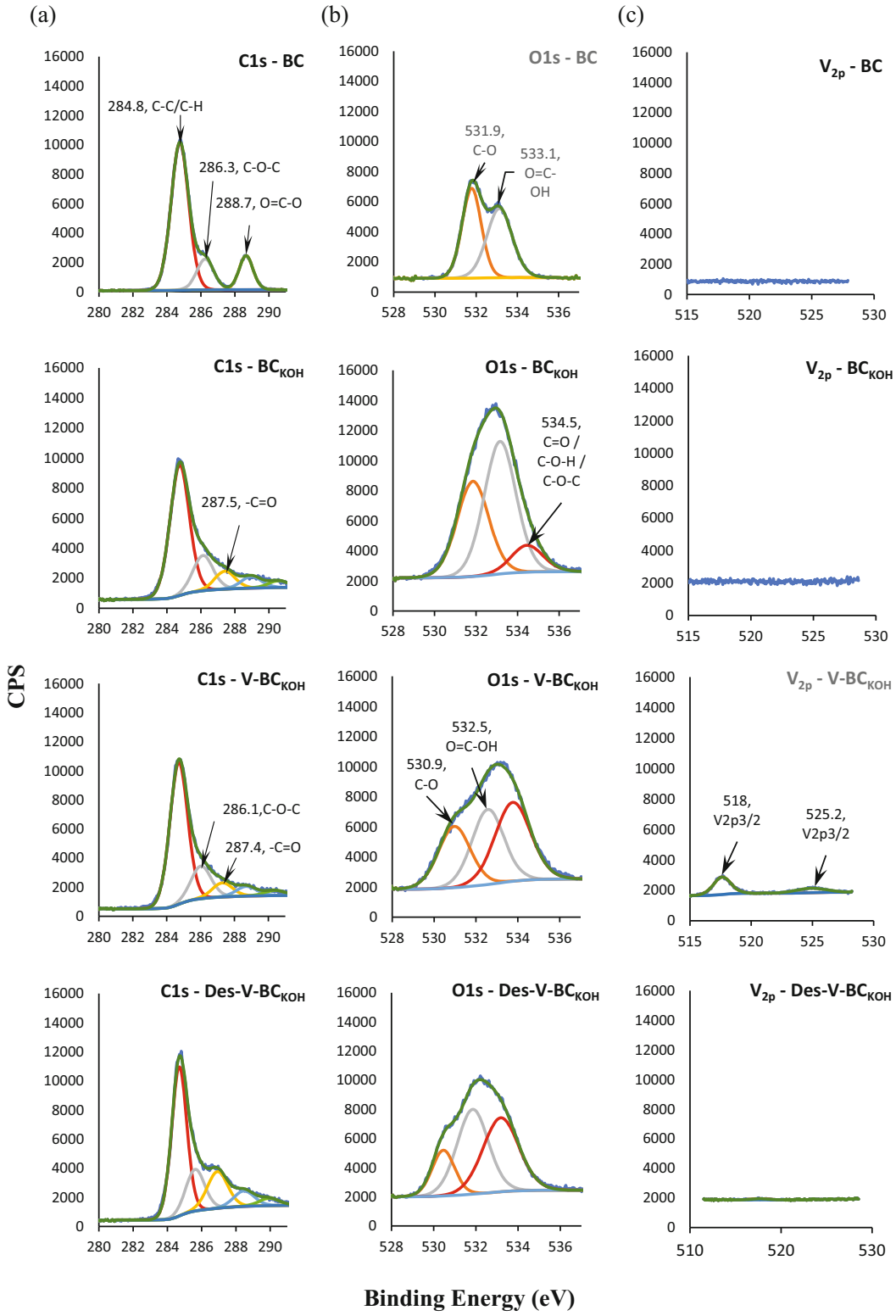

Figure 4. High-resolution XPS scans for the (a) C 1s, (b) O 1s and (c) V 2p regions of BC, BC_{KOH}, V-BC_{KOH} and Des-V-BC_{KOH}.

$$Bt = \left(\sqrt{\pi} - \sqrt{\pi - \frac{\pi^2 F(t)}{3}}\right)^2, \text{for } F(t) \le 0.85 \quad (7)$$

where Bt is Boyd's number and $F(t) = q/q_e$ at time t.

Based on the Weber approach, the graph depicted in Fig. 6(c) outlines two linear segments in the overall plot indicating again that at least two processes influence the rate of the V(V) adsorption process. The Boyd model specifically assumes intra-particle diffusion is the rate-limiting step if a plot of Bt against contact time

Journal of Chemical Technology and Biotechnology published by John Wiley & Sons Ltd on behalf of Society of Chemical Industry (SCI).

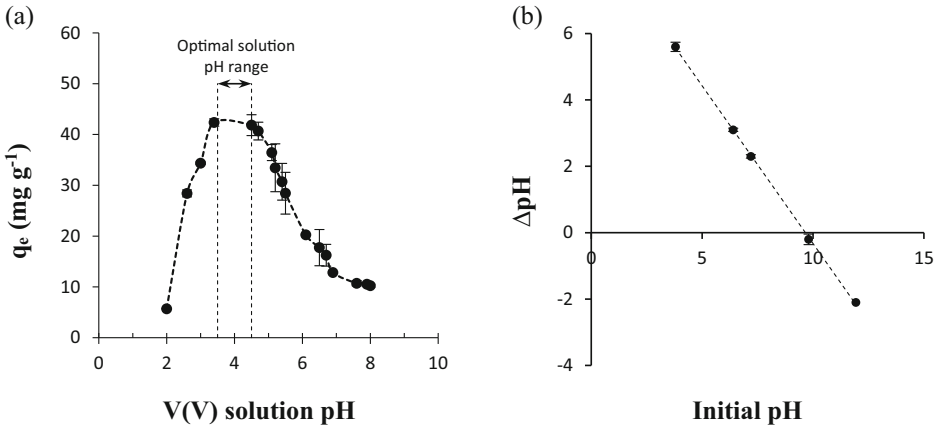

Figure 5. (a) Effect of solution pH on V(V) adsorption by BC_{KOH} using initial V(V) concentrations of 90 mg L^{-1} and 2 g L^{-1} of BC_{KOH} and (b) zero-point charge (pH_{pzc}) of BC_{KOH} at 293 K. Error bars indicate ±1 SD, $n = 3$.

yields a linear profile and passes through the origin. In the case of the first linear segment, a straight line is observed which passes through the origin indicating that the rate-limiting step can be considered to be diffusion of the V(V) species through the pores of BC_{KOH} to the binding sites on the adsorbent. Boyd also postulates that if the plot yields either a nonlinear profile or is linear but does not pass through the origin then the rate-limiting step can be considered to be the film diffusion step. Figure 6(b),(c) indicates that initially (up to about 30 min) the intra-particle diffusion is rate-controlling and thereafter film diffusion becomes the rate-controlling process, once the V(V) concentration gradient reduces across the film surrounding the adsorbent particles (i.e. as the solute concentration decreases).[60]

Adsorption

The plot of the equilibrium uptake of V(V) (q_e) *versus* equilibrium concentration (C_e) represents a type I isotherm curve as defined by the classification of Brunauer *et al.*,[66] whereby at low equilibrium adsorbate solution concentrations, uptake of V(V) is high and this is followed by the formation of an uptake plateau at higher equilibrium solution concentrations. Langmuir,[67] Freundlich[68] and Sips[69] isotherm models can be applied (Fig. 7) in assessing the adsorption process. The Langmuir model assumes an energetic equivalence of all binding sites on the adsorbent whereas the Freundlich isotherm model is based on the non-equivalence in energy terms of the binding sites and assumes a logarithmic relationship between the level of adsorption and equilibrium adsorbate solution concentration. The Sips model is a combined form of the Langmuir and Freundlich models which is expected to better predict the heterogeneity of the adsorption system. It approaches the Freundlich isotherm model at low concentrations and the Langmuir model at high concentrations. A nonlinear regression analysis was used to fit all three isotherm models (Eqns (8)–(10) respectively) to the experimental data where q_e and q_m (mg g^{-1}) are the experimental and the maximum adsorption capacities respectively, C_e (mg L^{-1}) is the equilibrium V(V) concentration in solution and K_L (L mg^{-1}) is the Langmuir constant relating to the adsorption energy. K_F (L g^{-1}) and n are Freundlich constants relating to adsorption capacity and adsorption energy, respectively, and K_s (L g^{-1}), α_s (L mg^{-1}) and β_s (exponent) are the Sips isotherm model constants.

$$q_e = \frac{q_m K_L C_e}{1 + K_L} \tag{8}$$

$$q_e = K_F C_e^{1/n} \tag{9}$$

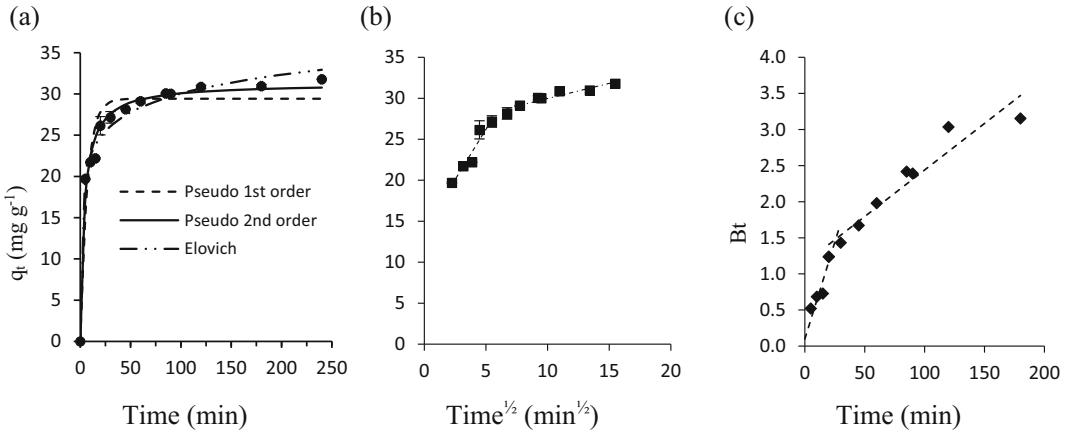

Figure 6. Fits of the sorption kinetic data of V(V) onto KOH-modified hydrochar using (a) PFO, PSO and Elovich equations, (b) intra-particle diffusion model and (C) Boyd model. All experiments ($n = 3$) were carried out at 293 K and solution pH 4. Error bars indicate ±1 SD, $n = 3$.

Journal of Chemical Technology and Biotechnology published by John Wiley & Sons Ltd on behalf of Society of Chemical Industry (SCI).

Table 3. Kinetics of V(V) adsorption onto BC_{KOH} using the PFO, PSO, Elovich, intra-particle diffusion and Boyd approaches at 293 K

Model	Parameters	Values
PFO	q_e (mg g^{-1})	29.42
	k_1 (min^{-1})	−0.145
	R^2	0.742
	χ^2	2.605
PSO	q_e (mg g^{-1})	31.29
	k_2 (g mg^{-1} min^{-1})	0.008
	R^2	0.924
	χ^2	0.650
Elovich	α (mg g^{-1} min^{-1})	300.4
	β (mg mg^{-1})	0.30
	R^2	0.940
	χ^2	0.396
Intra-particle diffusion	$k_{i,1}$ (mg g^{-1} $min^{-1/2}$)	2.446
	c_1 (mg g^{-1})	13.98
	R_1^2	0.920
	$k_{i,2}$ (mg g^{-1} $min^{-1/2}$)	0.369
	c_2 (mg g^{-1})	26.28
	R_2^2	0.891
Boyd	R_1^2 ($t \le 30$ min)	0.910
	R_2^2 ($t > 30$ min)	0.916

Table 4. Langmuir, Freundlich and Sips isotherm model parameters for V(V) adsorption on BC_{KOH} at 293 K

Model	Parameters	Values
Langmuir	q_m (mg g^{-1})	48.83
	K_L (L mg^{-1})	0.373
	R^2	0.929
	χ^2	13.66
Freundlich	K_F (mg g^{-1}) (mg $L^{-1})^{-1}$	17.32
	n	3.909
	R^2	0.826
	χ^2	32.95
Sips	K_s (L g^{-1})	6.641
	α_s (L mg^{-1})	0.146
	β_s	2.096
	R^2	0.960
	χ^2	596.75

$$q_e = \frac{K_s C_e^{\beta_s}}{1 + \alpha_s C_e^{\beta_s}} \quad (10)$$

As depicted in Fig. 7, the modelled Langmuir and Sips plots show close correlation with the experimental findings, while the Freundlich model was not as well correlated (Table 4). Saturation coverage (q_{max}) of V(V) on BC_{KOH} was estimated to be 48.83 mg g^{-1}. The Langmuir and Sips models yielded higher correlation coefficients (R^2 = 0.929 and 0.960 respectively) than the Freundlich approach (R^2 = 0.826), with the Langmuir model having a lower χ^2 value than the Sips model. This V(V) uptake level in the current study can be compared and contextualised with the results of other similar research studies in which an oxygen-doped biochar derived from pinewood sawdust[36] yielded a V(V) adsorption level of 70 mg g^{-1}, a red mud-modified sawdust biochar[12] yielded and uptake level of 16.45 mg g^{-1} and a nano zero-valent iron-modified biochar[29] yielded an uptake level of 48.5 mg g^{-1}.

Further assessment of the nature and applicability of the Langmuir adsorption process was carried out using the separation factor (R_L).[70] This factor is defined in Eqn (11), where K_L is the Langmuir constant for the V(V) adsorption process on BC_{KOH} (L mg^{-1}) and C_o is the initial V(V) concentration in solution (mg L^{-1}). An $R_L = 0$ suggests irreversible adsorption. If the situation $0 < R_L < 1$ pertains, then the adsorption process is considered to be suitable and potentially reversible. If $R_L = 1$, it can be assumed that a linear relationship exists between V(V) uptake and V(V) initial solution concentration. When $R_L > 1$, the V(V) adsorption process is unfavourable.

$$R_L = \frac{1}{(1 + K_L C_o)} \quad (11)$$

Figure 8(a) outlines the relationship between the initial V(V) solution concentrations and their associated separation factors

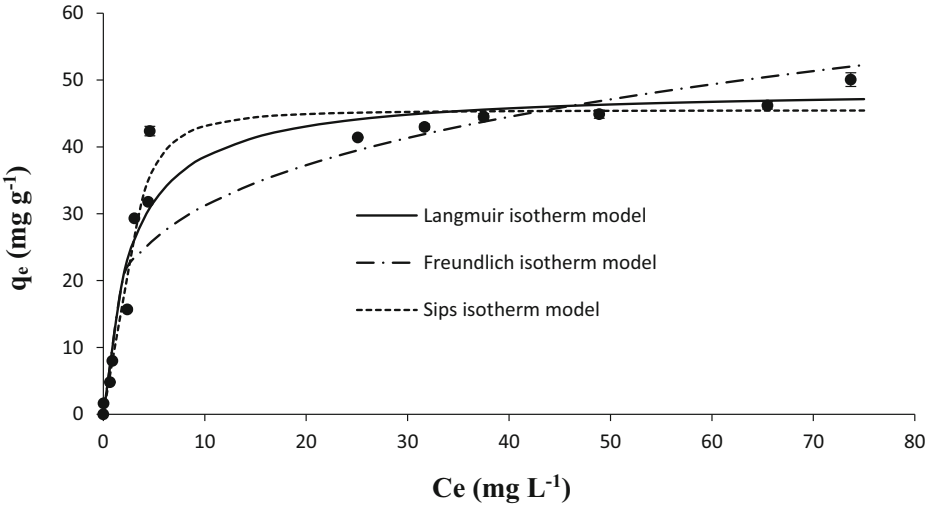

Figure 7. Langmuir, Freundlich and Sips isotherm models fitted to adsorption data of V(V) solution onto BC_{KOH}. Error bars indicate ±1 SD, n = 3.

Journal of Chemical Technology and Biotechnology published by John Wiley & Sons Ltd on behalf of Society of Chemical Industry (SCI).

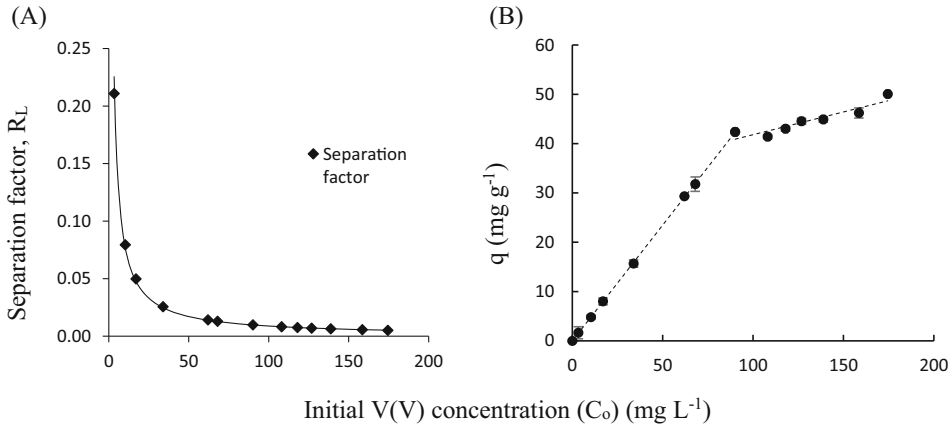

Figure 8. Plots of initial V(V) concentrations *versus* (a) Langmuir separation factor R_L and (b) measured adsorption rates. All experiments ($n = 3$) were carried out at solution pH 4, 293 K and 180 min contact time. Error bars indicate ±1 SD.

(R_L). All R_L values lie between 0 and 1 for the Langmuir model indicating the suitability of the V(V) adsorption process. At low initial V(V) adsorption solution concentrations (0–35 mg L^{-1}), the R_L values range from 0.21 to 0.03 constituting a favourable V(V) uptake scenario. Further increase in initial V(V) adsorption solution concentrations (35–175 mg L^{-1}) yields a more constant set of R_L values ranging from 0.03 to 0.01 indicating continued and strengthened adsorption of V(V) on BC_{KOH}.

A linear and rapidly increasing adsorption level was observed as the V(V) concentration increased and this plateaued to approximately 45 mg g^{-1} at a V(V) concentration of approx. 100 mg L^{-1} (Fig. 8(b)), indicating either possible complete pore volume or binding site saturation.

Thermodynamics

The uptake of V(V) on BC_{KOH} decreased in a linear manner as a function of increasing temperature (Fig. 9(a)). Over the adsorption temperature range from 293 to 343 K, V(V) uptake level decreased in a consistent manner from approximately 36.2 to 30.7 mg g^{-1}. This reduction in uptake with increased temperature is indicative of an exothermic adsorption process and a weakening of the interaction between V(V) and the BC_{KOH} surface binding sites. Equations (12)–(15) were used to estimate the thermodynamic parameters for the adsorption process. K_c and ΔG° were calculated (Eqns (12) and (13) respectively), while ΔS° and ΔH° are obtained from the intercept and slope respectively of a plot of ln K *versus* $1/T$ (Fig. 9(b)).

$$K_c = \frac{C_o - C_e}{C_e} \tag{12}$$

$$\Delta G^\circ = -RT \ln K_c \tag{13}$$

$$\Delta G^\circ = \Delta H^\circ - T\Delta S^\circ \tag{14}$$

$$\ln K = \frac{\Delta S^\circ}{R} - \frac{\Delta H^\circ}{RT} \tag{15}$$

where K_c is the thermodynamic equilibrium constant, C_o (mg L^{-1}) and C_e (mg L^{-1}) are the initial and equilibrium V(V) concentrations respectively, R (8.314 J mol^{-1} K^{-1}) is the gas constant and T (K) is the temperature of the adsorption process.[71]

From Table 5, it is observed that the Gibbs free energy change accompanying the adsorption process at all five experimental temperatures is negative confirming the spontaneity of the V(V) adsorption process. At 293 K, the value ΔG° is −8.24 kJ mol^{-1} while at 343 K, the value of ΔG° reduces to −5.03 kJ mol^{-1} indicating a reduction in spontaneity of the V(V) adsorption process onto BC_{KOH} with increasing temperature. The negative enthalpy change (ΔH° = −25.97 kJ mol^{-1}) indicates that the adsorption

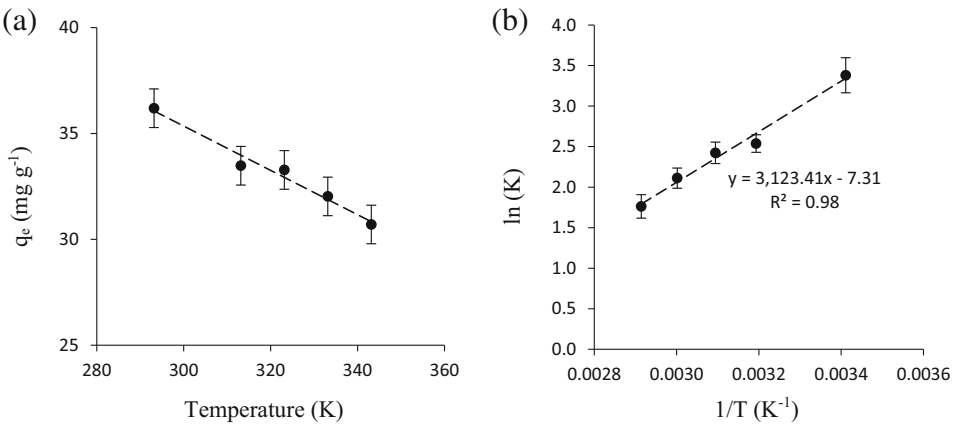

Figure 9. (a) Effect of temperature on uptake of V(V) onto BC_{KOH} for initial V(V) concentrations of 90 mg L^{-1}, BC_{KOH} dosage rate of 2 g L^{-1} and pH 4. (b) Arrhenius plot for adsorption of V(V) onto BC_{KOH} at 293–343 K. Error bars indicate ±1 SD, $n = 3$.

Journal of Chemical Technology and Biotechnology published by John Wiley & Sons Ltd on behalf of Society of Chemical Industry (SCI).

Table 5. Thermodynamic parameters ($n = 3$, $\Delta G°$ given as mean ± SD) for the adsorption of V(V) onto BC_{KOH} for temperature range 293–343 K.

Temperature (K)	Thermodynamic parameters			
	K_c	$\Delta G°$ (kJ mol^{-1})	$\Delta H°$ (kJ mol^{-1})	$\Delta S°$ (J mol^{-1} K^{-1})
293	29.37	−8.24 ± 0.03	−25.97	−60.79
313	12.68	−6.61 ± 0.07		
323	11.25	−6.51 ± 0.03		
333	12.68	−5.85 ± 0.12		
343	29.37	−5.03 ± 0.02		

process is exothermic with heat release accompanying the binding process and is favoured by lower temperatures. This enthalpy change value suggests that V(V) adsorption is most likely a physisorption process. The Gibbs free energy and enthalpy changes compare with the research of others where the biosorption of V(V) onto H_3PO_4-modified *Lantana camara* biochar and a red mud-modified sawdust biochar, both in an endothermic adsorption process, yielded thermodynamic parameter values of ($\Delta G° = -7.20$ kJ mol^{-1} and $\Delta H° = +46.17$ kJ mol^{-1})[29] and ($\Delta G° = -0.27$ kJ mol^{-1} and $\Delta H° = +24.5$ kJ mol^{-1})[10] respectively. The negative value of the entropy change ($\Delta S° = -60.78$ J mol^{-1} K^{-1}) suggests an increased orderliness at the solid–solution interface during adsorption of V(V).

Influence of ionic strength

Waste streams often contain a range of cations at significantly varying concentrations.[72] The sodium cation (Na^+) can often be present in high concentrations relative to V(V), and this presents a potential difficulty in the successful adsorption of V(V) from waste streams.[73] The potential influence of saline concentration and particularly the possibility of high sodium cation (Na^+) concentrations competing with V(V) for binding sites on BC_{KOH} were evaluated. Figure 10 indicates that in the absence of Na^+ content in the adsorption solution, the uptake level of V(V) was 42.4 mg g^{-1}. As the Na^+ content was increased to 100 mg L^{-1}, the level of V(V) uptake dropped to approximately 30.5 mg g^{-1}. Thereafter, as the Na^+ ion content in solution was increased in successive steps to 400 mg L^{-1}, only a minimal reduction in V(V) uptake was observed. This suggests that, with the initial introduction of Na^+ content to the adsorption solution, the sites on the surface of BC_{KOH} may either be protonated with H^+ or be bound with Na^+ at acidic solution pH values. This may lead to an initial reduction in V(V) binding but, once equilibrium is established between the surface H^+ and Na^+, the residual V(V) adsorption level remains relatively constant. Hence, it can be concluded that the presence of Na^+ levels and saline content in the adsorption solution does lead to some level of reduction in V(V) adsorption but increasing Na^+ concentrations produce only a slight reduction in V(V) adsorption thereafter.

Other researchers have studied the influence of saline levels on the adsorption of a number of cations (Cd, Cr, Cu, Ni and Pb) onto a range of low-cost adsorbents including coconut coir fibre, biochar and an iron-coated biochar[74] and found that ionic strength (NaCl) had no real impact on cation removal levels, whereas studies of the sorption of Ni(II) on GMZ bentonite suggested that the Ni(II) uptake level in the presence of $NaClO_4$ was clearly dependent on ionic strength particularly at acidic pH values.[75]

Recovery of V(V) and adsorbent re-use

Metals such as V(V) and Ga(II) are valuable[76] and while often at low concentrations in wastewaters, it is important to effect their recovery for both environmental and economic reasons.[77] While some adsorbents and adsorption systems have been tested in the removal of V(V) from waste streams, it is imperative to find an adsorbent which can not only effectively remove V(V) from solution but also facilitate desorption and recovery of the adsorbed V(V) content over a series of cycles.

Figure 11 illustrates the V(V) adsorption and recovery profiles over a three-cycle experiment using 2 mol L^{-1} KOH as the desorbing/regenerating agent. Using an initial V(V) adsorption solution concentration of approximately 95 mg L^{-1}, each cycle showed full regeneration of the BC_{KOH} adsorbent following treatment with 2 mol L^{-1} KOH and no loss of subsequent V(V) uptake capacity as evidenced by a continued and consistent level of V(V) adsorption in the range 42–46 mg g^{-1}. The integrity of the BC_{KOH} adsorbent and V(V) adsorption process remained largely unaltered from cycle 1 to cycle 3.

The results of the regeneration studies confirm the nature of the adsorption process as being a type of physisorption process with a relatively weak binding interaction between V(V) and the BC_{KOH} adsorbent. Whilst there is only limited research available specifically in terms of V(V) desorption from biochars, some researchers have used varying concentrations of a range of desorbing agents in the desorption of V(V). Table 6 outlines the results of this research in the context of some of these studies where many

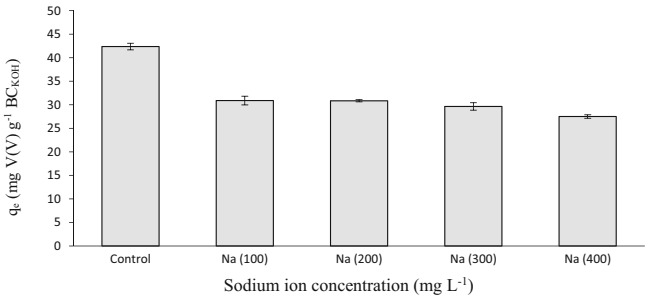

Figure 10. Effect of Na^+ solution concentration on V(V) adsorption onto BC_{KOH}. V(V) concentrations were 90 mg L^{-1}, BC_{KOH} application rate was 2 g L^{-1}, pH 3.5, contact time was 180 min and temperature was 293 K. Error bars indicate ±1 SD, $n = 3$.

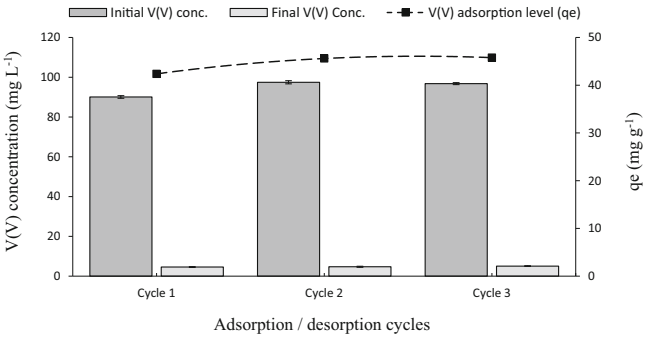

Figure 11. Regeneration of BC_{KOH} using 2 mol L^{-1} KOH and its impacts on V(V) adsorption level over three cycles. Error bars indicate ±1 SD, $n = 3$.

Journal of Chemical Technology and Biotechnology published by John Wiley & Sons Ltd on behalf of Society of Chemical Industry (SCI).

Table 6. Selected V(V) desorption studies and typical desorbing agents

Adsorbent	Regenerant	Time (min)	Recovery (%)
Modified pine bark[31]	4 mol L^{-1} NaCl	30	80
Activated carbon[78]	2.5 mol L^{-1} NaOH	—	93.7–95.6
Amine-functionalised poly-grafted tamarind fruit shell[79]	0.2 mol L^{-1} NaOH	240	83.8
KOH-modified seaweed biochar (current study)	2 mol L^{-1} KOH	120	94.9

are based on the use of varying concentrations of NaOH with recovery levels in excess of 80%.

The ultimate use of spent and end-of-use KOH-modified seaweed biochar presents some potential environmental issues. Given the nature of KOH treatment in the preparation process, the surface properties and specific organic functional group moieties together with inorganic components may have some impact on any receiving substrate or soil. In particular, the waste biochar, following treatment with KOH, has the potential to alter the pH of soil or a particular medium. This ultimately may result in certain chemical reactions between the modified biochar and the application environment leading to a potential release of toxic components.[80]

CONCLUSIONS

The removal of V(V) from aqueous solution was carried in a batch process using BC_{KOH}. Initially the physical and chemical characteristics of BC_{KOH} were evaluated and clear evidence in the form of FTIR, EDX and XPS findings indicated that the surface of the biochar had developed new forms of oxygenated species following the KOH modification process. The V(V) adsorption process was assessed as a function of initial V(V) solution concentration, solution pH, V(V) contact time, temperature and solution ionic strength. V(V) uptake on BC_{KOH} was heavily influenced by solution pH with an optimum range between pH 3.5 and 4.5. The adsorption process, exothermic in nature ($\Delta H^{\circ} = -25.7$ kJ mol^{-1} at 293 K), was favoured by lower temperatures and the magnitude of this enthalpy change suggests that the binding process was physisorption in nature. The presence of high ionic strength in the adsorption solution leads to an initial reduction in V(V) uptake with a levelling off in impact thereafter at higher ionic strengths. Under optimal conditions, maximum V(V) adsorption level on BC_{KOH} reached 48.83 mg g^{-1} and the nature of the adsorption process was best described by the Langmuir model. Of key concern with any adsorption process is its ease of reversibility. The action of 2 mol L^{-1} KOH, as desorbing agent, proved effective in reversing the adsorption process, thereby permitting desorption of the bound V(V), regeneration of the BC_{KOH} adsorbent and re-adsorption of a consistently high-level V(V) uptake over three successive cycles. Based on the outcomes from this research work, BC_{KOH} offers clear potential to be used as a cost-effective adsorbent in the context of a range of acidic industrial waste streams. Future work should aim to develop a continuous flow process to further develop its potential in an industrial setting and inform future economic and ecological assessment.

ACKNOWLEDGEMENTS

This work was supported by the Geological Survey of Ireland (GSI, project no. 2018-ERAMIN2-002), the Irish Environmental Protection Agency (EPA) and an EU ERA-MIN2 award to the EU Biomimic Consortium (ID 86).

DATA AVAILABILITY STATEMENT

The data that support the finding of this study are available upon reasonable request from the corresponding author.

REFERENCES

1 Hou M, Li M, Yang X and Pan R, Responses of nonprotein thiols to stress of vanadium and mercury in maize (*Zea mays* L.) seedlings. *Bull Environ Contam Toxicol* **102**:425–431 (2019).
2 Imtiaz M, Rizwan MS, Xiong S, Li H, Ashraf M, Shahzad SM *et al.*, Vanadium, recent advancements and research prospects: a review. *Environ Int* **80**:79–88 (2015).
3 Li HY, Yang Y, Zhang M, Wei W and Xie B, A novel anion exchange method based on in situ selectively reductive desorption of Cr(VI) for its separation from V(V): toward the comprehensive use of hazardous wastewater. *J Hazard Mater* **368**:670–679 (2019).
4 Li HY, Fang HX, Wang K, Zhou W, Yang Z, Yan XM *et al.*, Asynchronous extraction of vanadium and chromium from vanadium slag by stepwise sodium roasting–water leaching. *Hydrometallurgy* **156**:124–135 (2015).
5 Hua M, Zhang S, Pan B, Zhang W, Lv L and Zhang Q, Heavy metal removal from water/wastewater by nanosized metal oxides: a review. *J Hazard Mater* **211**:317–331 (2012).
6 Zhang B, Feng C, Ni J, Zhang J and Huang W, Simultaneous reduction of vanadium(V) and chromium(VI) with enhanced energy recovery based on microbial fuel cell technology. *J Power Sources* **204**:34–39 (2012).
7 Nguyen TH and Lee MS, Solvent extraction of vanadium(V) from sulfate solutions using LIX 63 and PC 88A. *J Ind Eng Chem* **31**:118–123 (2015).
8 Zhang B, Hao L, Tian C, Yuan S, Feng C, Ni J *et al.*, Microbial reduction and precipitation of vanadium(V) in groundwater by immobilized mixed anaerobic culture. *Bioresour Technol* **192**:410–417 (2015).
9 Watt JA, Burke IT, Edwards RA, Malcolm HM, Mayes WM, Olszewska JP *et al.*, Vanadium: a re-emerging environmental hazard. *Environ Sci Technol* **52**:11973–11974 (2018).
10 Huang JH, Huang F, Evans L and Glasauer S, Vanadium: global (bio) geochemistry. *Chem Geol* **417**:68–89 (2015).
11 Fang D, Zhang X, Dong M and Xue X, A novel method to remove chromium, vanadium and ammonium from vanadium industrial wastewater using a byproduct of magnesium-based wet flue gas desulfurization. *J Hazard Mater* **336**:8–20 (2017).
12 Ghanim B, Murnane JG, O'Donoghue L, Courtney R, Pembroke JT and O'Dwyer TF, Removal of vanadium from aqueous solution using a red mud modified saw dust biochar. *J Water Process Eng* **33**: 101076 (2020).
13 Gomes HI, Mayes WM, Baxter HA, Jarvis AP, Burke IT, Stewart DI *et al.*, Options for managing alkaline steel slag leachate: a life cycle assessment. *J Clean Prod* **202**:401–412 (2018).
14 Li HY, Li C, Zhang M, Wang K and Xie B, Removal of V(V) from aqueous Cr(VI)-bearing solution using anion exchange resin: equilibrium and kinetics in batch studies. *Hydrometallurgy* **165**:381–389 (2016).
15 Yi L, Shen X, Shu Y, Deng B, Zhong Q, Peng Z *et al.*, Application of biomass energy in titanomagnetite reduction for Fe/Ti recycling: overcoming the challenge of iron grain growth. *Fuel* **388**:134511 (2025).
16 Zhang B, Qiu R, Lu L, Chen X, He C, Lu J *et al.*, Autotrophic vanadium(V) bioreduction in groundwater by elemental sulfur and zerovalent iron. *Environ Sci Technol* **52**:7434–7442 (2018).
17 Hao L, Liu Y, Chen N, Hao X, Zhang B and Feng C, Microbial removal of vanadium(V) from groundwater by sawdust used as a sole carbon source. *Sci Total Environ* **751**:142161 (2021).

18 Zhao Z, Long H, Li X, Fan Y and Han Z, Precipitation of vanadium from Bayer liquor with lime. *Hydrometallurgy* **115**:52–56 (2012).
19 Yang X, Zhang Y and Bao S, Preparation of high purity V_2O_5 from a typical low-grade refractory stone coal using a pyro-hydrometallurgical process. *Minerals* **6**:69 (2016).
20 Rout PC and Sarangi K, Separation of vanadium using both hollow fiber membrane and solvent extraction technique: a comparative study. *Sep Purif Technol* **122**:270–277 (2014).
21 Crini G and Lichtfouse E, Advantages and disadvantages of techniques used for wastewater treatment. *Environ Chem Lett* **1**:145–155 (2019).
22 Li Y, Yu H, Liu L and Yu H, Application of co-pyrolysis biochar for the adsorption and immobilization of heavy metals in contaminated environmental substrates. *J Hazard Mater* **420**:126655 (2021).
23 Polowczyk I, Cyganowski P, Urbano BF, Rivas BL, Bryjak M and Kabay N, Amberlite IRA-400 and IRA-743 chelating resins for the sorption and recovery of molybdenum(VI) and vanadium(V): equilibrium and kinetic studies. *Hydrometallurgy* **1**:496–507 (2017).
24 Zhu X, Li W, Zhang Q, Zhang C and Chen L, Separation characteristics of vanadium from leach liquor of red mud by ion exchange with different resins. *Hydrometallurgy* **176**:42–48 (2018).
25 Leiviskä T, Khalid MK, Sarpola A and Tanskanen J, Removal of vanadium from industrial wastewater using iron sorbents in batch and continuous flow pilot systems. *J Environ Manag* **190**:231–242 (2017).
26 Kong X, Chen J, Tang Y, Lv Y, Chen T and Wang H, Enhanced removal of vanadium(V) from groundwater by layered double hydroxide-supported nanoscale zerovalent iron. *J Hazard Mater* **392**:122392 (2020).
27 Wang F, Qi X, Zhang H and Yang Z, Innovative molten salt techniques for biomass valorization: transforming biomass into advanced carbon materials. *Carbon* **234**:119999 (2025).
28 Xu Y, Fan Z, Li X, Yang S, Wang J, Zheng A *et al.*, Cooperative production of monophenolic chemicals and carbon adsorption materials from cascade pyrolysis of acid hydrolysis lignin. *Bioresour Technol* **399**: 130557 (2024).
29 Fan C, Chen N, Qin J, Yang Y, Feng C, Li M *et al.*, Biochar stabilized nano zero-valent iron and its removal performance and mechanism of pentavalent vanadium (V(V)). *Colloids Surf A* **599**:124882 (2020).
30 Niu HC and Volesky B, Biosorption of chromate and vanadate species with waste crab shells. *Hydrometallurgy* **84**:28–36 (2006).
31 Zhang R and Leiviskä T, Surface modification of pine bark with quaternary ammonium groups and its use for vanadium removal. *Chem Eng J* **385**:123967 (2020).
32 Iamsaard K, Weng CH, Yen LT, Tzeng JH, Poonpakdee C and Lin YT, Adsorption of metal on pineapple leaf biochar: key affecting factors, mechanism identification, and regeneration evaluation. *Bioresour Technol* **344**:126131 (2022).
33 Tyagi U, Enhanced adsorption of metal ions onto *Vetiveria zizanioides* biochar via batch and fixed bed studies. *Bioresour Technol* **345**: 126475 (2022).
34 Shan R, Shi Y, Gu J, Wang Y and Yuan H, Single and competitive adsorption affinity of heavy metals toward peanut shell-derived biochar and its mechanisms in aqueous systems. *Chin J Chem Eng* **28**: 1375–1383 (2020).
35 Chen K, Ma D, Yu H, Zhang S, Seyler BC, Chai Z *et al.*, Biosorption of V(V) onto *Lantana camara* biochar modified by H_3PO_4: characteristics, mechanism, and regenerative capacity. *Chemosphere* **291**:132721 (2022).
36 Wu B, Ifthikar J, Oyekunle DT, Jawad A, Chen Z, Chen Z *et al.*, Interpret the elimination behaviors of lead and vanadium from the water by employing functionalized biochars in diverse environmental conditions. *Sci Total Environ* **789**:148031 (2021).
37 Yu YQ, Li JX, Liao YL and Yang JY, Effectiveness, stabilization, and potential feasible analysis of a biochar material on simultaneous remediation and quality improvement of vanadium contaminated soil. *J Clean Prod* **277**:123506 (2020). https://doi.org/10.1016/j.jclepro.2020.123506.
38 He R, Neupane M, Zia A, Huang X, Bowers C, Wang M *et al.*, Binder-free wood converted carbon for enhanced water desalination performance. *Adv Funct Mater* **32**:2208040 (2022). https://doi.org/10.1002/adfm.202208040.
39 Shan L, Zhang Y, Xu Y, Gao M, Xu T and Si C, Wood-based hierarchical porous nitrogen-doped carbon/manganese dioxide composite electrode materials for high-rate supercapacitor. *Adv Compos Hybrid Mater* **6**:174 (2023). https://doi.org/10.1007/s42114-023-00744-y.
40 Méndez A, Gascó G, Ruiz B and Fuente E, Hydrochars from industrial macroalgae '*Gelidium Sesquipedale*' biomass wastes. *Bioresour Technol* **275**:386–393 (2019). https://doi.org/10.1016/j.biortech.2018.12.074.
41 Ghanim B, O'Dwyer TF, Leahy JJ, Willquist K, Courtney R, Pembroke JT *et al.*, Application of KOH modified seaweed hydrochar as a biosorbent of vanadium from aqueous solution: characterisations, mechanisms and regeneration capacity. *J Environ Chem Eng* **8**:104176 (2020). https://doi.org/10.1016/j.jece.2020.104176.
42 Wang Z, Liu G, Zheng H, Li F, Ngo HH, Guo W *et al.*, Investigating the mechanisms of biochar's removal of lead from solution. *Bioresour Technol* **177**:308–317 (2015).
43 Kończyk J, Kluziak K and Kołodyńska D, Adsorption of vanadium(V) ions from the aqueous solutions on different biomass-derived biochars. *J Environ Manag* **313**:114958 (2022).
44 Keiluweit M, Nico PS, Johnson MG and Kleber M, Dynamic molecular structure of plant biomass-derived black carbon (biochar). *Environ Sci Technol* **44**:1247–1253 (2010).
45 Cantrell KB, Hunt PG, Uchimiya M, Novak JM and Ro KS, Impact of pyrolysis temperature and manure source on physicochemical characteristics of biochar. *Bioresour Technol* **107**:419–428 (2012).
46 Reguyal F and Sarmah AK, Adsorption of sulfamethoxazole by magnetic biochar: effects of pH, ionic strength, natural organic matter and 17α-ethinylestradiol. *Sci Total Environ* **628**:722–730 (2018).
47 Cai Y, Wang X, Feng J, Zhu M, Alsaedi A, Hayat T *et al.*, Fully phosphorylated 3D graphene oxide foam for the significantly enhanced U(VI) sequestration. *Environ Pollut* **249**:434–442 (2019).
48 Ahmed W, Xu T, Mahmood M, Núñez-Delgado A, Ali S, Shakoor A *et al.*, Nano-hydroxyapatite modified biochar: insights into the dynamic adsorption and performance of lead(II) removal from aqueous solution. *Environ Res* **214**:113827 (2022).
49 O'Connell DW, Aszalos B, Birkinshaw C and O'Dwyer TF, A study of the mechanisms of divalent copper binding to a modified cellulose adsorbent. *J Appl Polym Sci* **116**:2496–2503 (2010).
50 Yang C, Yao Q, Li L, Xiao X, Lu L, Liu C *et al.*, The isolated Ca-Nx sites in biochar boosting Fe catalyzed Fenton-like oxidation of tris(2-chloroethyl) phosphate: properties, mechanisms, and applications. *Appl Catal B Environ Energy* **366**:125056 (2025).
51 Tang Q, Shi C, Shi W, Huang X, Ye Y, Jiang W *et al.*, Preferable phosphate removal by nano-La(III) hydroxides modified mesoporous rice husk biochars: role of the host pore structure and point of zero charge. *Sci Total Environ* **662**:511–520 (2019).
52 Hernández L, Araujo ML, Madden W, Del Carpio E, Lubes V and Lubes G, Vanadium complexes with polypyridyl ligands: speciation, structure and potential medicinal activity. *J Inorg Biochem* **229**: 111712 (2022).
53 Burakov AE, Galunin EV, Burakova IV, Kucherova AE, Agarwal S, Tkachev AG *et al.*, Adsorption of heavy metals on conventional and nanostructured materials for wastewater treatment purposes: a review. *Ecotoxicol Environ Saf* **148**:702–712 (2018).
54 Baldermann A and Stamm FM, Effect of kinetics, pH, aqueous speciation and presence of ferrihydrite on vanadium(V) uptake by allophanic and smectitic clays. *Chem Geol* **607**:121022 (2022).
55 Gowda SA, Goveas LC and Dakshayini K, Adsorption of methylene blue by silver nanoparticles synthesized from *Urena lobata* leaf extract: kinetics and equilibrium analysis. *Mater Chem Phys* **288**:126431 (2022).
56 Sherugar P, Padaki M, Naik NS, George SD and Murthy DH, Biomass-derived versatile activated carbon removes both heavy metals and dye molecules from wastewater with near-unity efficiency: mechanism and kinetics. *Chemosphere* **287**:132085 (2022).
57 Wu FC, Tseng RL and Juang RS, Characteristics of Elovich equation used for the analysis of adsorption kinetics in dye-chitosan systems. *Chem Eng J* **150**:366–373 (2009). https://doi.org/10.1016/j.cej.2009.01.014.
58 Weber WJ Jr and Morris JC, Kinetics of adsorption on carbon from solution. *J Sanit Eng Div* **89**:31–59 (1963).
59 Boyd GE, Adamson AW and Myers LS Jr, The exchange adsorption of ions from aqueous solutions by organic zeolites. II. Kinetics. *J Am Chem Soc* **69**:2836–2848 (1947).
60 Ghanim B, Leahy JJ, O'Dwyer TF, Kwapinski W, Pembroke JT and Murnane JG, Removal of hexavalent chromium (Cr(VI)) from aqueous solution using acid-modified poultry litter-derived hydrochar: adsorption, regeneration and reuse. *J Chem Technol Biotechnol* **97**: 55–66 (2022). https://doi.org/10.1002/jctb.6904.

Journal of Chemical Technology and Biotechnology published by John Wiley & Sons Ltd on behalf of Society of Chemical Industry (SCI).

61 Omidinasab M, Rahbar N, Ahmadi M, Kakavandi B, Ghanbari F, Kyzas GZ *et al*., Removal of vanadium and palladium ions by adsorption onto magnetic chitosan nanoparticles. *Environ Sci Pollut Res* **25**: 34262–34276 (2018).
62 Behnamfard A and Salarirad MM, Equilibrium and kinetic studies on free cyanide adsorption from aqueous solution by activated carbon. *J Hazard Mater* **170**:127–133 (2009).
63 Sahoo TR and Prelot B, Adsorption processes for the removal of contaminants from wastewater: the perspective role of nanomaterials and nanotechnology, in *Nanomaterials for the Detection and Removal of Wastewater Pollutants*. Elsevier, Amsterdam, Netherlands, pp. 161–222 (2020).
64 Sun F, Liu M, Yuan B, He J, Wu P, Liu C *et al*., Separation of vanadium and chromium by selective adsorption by titanium-based microspheres. *Chem Eng J* **450**:138039 (2022).
65 Reichenberg D, Properties of ion-exchange resins in relation to their structure. III. Kinetics of exchange. *J Am Chem Soc* **75**:589–597 (1953).
66 Brunauer S, Deming LS, Deming E and Teller E, On a theory of the van der Waals adsorption of gases. *J Am Chem Soc* **62**:1723–1732 (1940).
67 Langmuir I, The adsorption of gases on plane surfaces of glass, mica and platinum. *J Am Chem Soc* **40**:1361–1403 (1918).
68 Freundlich H, Adsorption. *J Phys Chem* **7**:57–64 (1926).
69 Sips R, On the structure of a catalyst surface. *J Chem Phys* **16**:490–495 (1948). https://doi.org/10.1063/1.1746922.
70 Wang S, Nam H and Nam H, Preparation of activated carbon from peanut shell with KOH activation and its application for H_2S adsorption in confined space. *J Environ Chem Eng* **8**:103683 (2020).
71 Argun ME, Dursun S, Ozdemir C and Karatas M, Heavy metal adsorption by modified oak sawdust: thermodynamics and kinetics. *J Hazard Mater* **141**:77–85 (2007).
72 Younis SA, El-Salamony RA, Tsang YF and Kim KH, Use of rice straw-based biochar for batch sorption of barium/strontium from saline water: protection against scale formation in petroleum/desalination industries. *J Clean Prod* **250**:119442 (2020).
73 Gomes HI, Mayes WM, Rogerson M, Stewart DI and Burke IT, Alkaline residues and the environment: a review of impacts, management practices and opportunities. *J Clean Prod* **112**:3571–3582 (2016).
74 Esfandiar N, Suri R and McKenzie ER, Competitive sorption of Cd, Cr, Cu, Ni, Pb and Zn from stormwater runoff by five low-cost sorbents; effects of co-contaminants, humic acid, salinity and pH. *J Hazard Mater* **423**:126938 (2022).
75 Yang S, Li J, Lu Y, Chen Y and Wang X, Sorption of Ni (II) on GMZ bentonite: effects of pH, ionic strength, foreign ions, humic acid and temperature. *Appl Radiat Isot* **67**:1600–1608 (2009).
76 Zhang B, Liu C, Liu Z, Li Z and Jiang M, Remediation of the vanadium slag processing residue and recovery of the valuable elements. *Process Saf Environ Prot* **128**:362–371 (2019).
77 Chen XM, Li HY, Wei CC, Cheng J, Diao J, Xie B *et al*., Selective chemical etching of vanadium slag enables highly efficient and clean extraction of vanadium. *ACS Sustain Chem Eng* **13**:1327–1335 (2025).
78 Keränen A, Leiviskä T, Salakka A and Tanskanen J, Removal of nickel and vanadium from ammoniacal industrial wastewater by ion exchange and adsorption on activated carbon. *Desalin Water Treat* **53**:2645–2654 (2015).
79 Anirudhan TS and Radhakrishnan PG, Adsorptive performance of an amine-functionalized poly(hydroxyethylmethacrylate)-grafted tamarind fruit shell for vanadium(V) removal from aqueous solutions. *Chem Eng J* **165**:142–150 (2010).
80 Xiang L, Liu S, Ye S, Yang H, Song B, Qin F *et al*., Potential hazards of biochar: the negative environmental impacts of biochar applications. *J Hazard Mater* **420**:126611 (2021).

